Spalling failure mechanism of a railway turnout made from carbide-free bainitic steel

LUO, Quanshun <http://orcid.org/0000-0003-4102-2129>, KITCHEN, Matthew, FARMILO, Nick, LI, Jianbin, LI, Wenbo and LI, Yanzheng

To be presented in 25th Int. Conf. Wear of Materials, Elsevier, Sitges, Spain, 13-17 April 2025

Spalling failure mechanism of a railway turnout made from carbide-free bainitic steel

Quanshun Luo[1], Matthew Kitchen[1], Nick Farmilo[1], Jianbin Li[2], Wenbo Li[3], Yanzheng Li[2]

[1] Materials and Engineering Research Institute, Sheffield Hallam University, Sheffield, UK
[2] China Railway High-Tech Industry Corporation Limited, Beijing, China
[3] China Railway Baoji Bridge Group Co. Ltd, Baoji, Shaanxi Province, China
Corresponding author: Dr Quanshun Luo, email: q.luo@shu.ac.uk. Presenting author: Dr Matthew Kitchen, email: m.kitchen@shu.ac.uk

Abstract

Railway turnouts play a transition role between straight and branching rails and therefore suffer from spalling failure as a result of repeated rolling contacts with wheels, as well as shear and impact loads. In this paper, we present a comprehensive failure investigation on the spalling failure mechanism of an off-track turnout made from bainitic steel. The experimental research was focused on the rolling-induced microstructural evolution from various depths to the rail top which caused the cracking and spalling wear. The worn turnout was analysed both on the rail top and on metallographically polished cross-sections using a variety of methods including optical microscopy, microhardness testing, field-emission scanning electron microscopy and energy dispersive X-ray spectroscopy, transmission electron microscopy, and quantitative X-ray diffraction for crystallography and surface residual stress analysis.

The results revealed that, the turnout was a low carbon and Si-Mn-Cr-Ni-Mo alloyed steel showing a dual-phase carbide-free microstructure of bainitic ferrite laths and retained inter-lath austenite. The rolling contact fatigue on the rail top resulted in the formation of spalling pits, cracking, extreme hardening, embrittlement, and the creation of a compressive stress of 400 MPa. The spalling failure was associated with a gradient microhardness profile to a depth of 1.5 mm, from $HV_{0.1}$ 7.3 GPa of the rail top to $HV_{0.1}$ 3.9 GPa of the bulk steel. Surface cracks were found to have propagated from the rail top to various depths up to 0.9 mm. The spalling failure was caused by deformation induced microstructure evolution within a depth of 200 μm from strain-free bainite to sub-micro and nano-scale laminates and eventually to quasi-amorphous rail top. Phenomena of transformation induced plasticity (TRIP) were found, not only including the decrease of retained austenite in the laminate structure, but also the formation of martensitic laths beneath the laminates.

Key Words

Spalling failures; Railway turnouts; Carbide-free bainitic steel; Rolling contact fatigue; Transformation induced plasticity (TRIP); Strain hardening and embrittlement

1 Introduction

In railway transportation, rails and related crossings and turnouts are subjected to dynamic rolling contact loads from the load-bearing wheels. With the demand to increase train speed and axle loads in modern transportation, high performance rail materials are demanded to maintain good performance and safety. Most rails are manufactured from high strength pearlitic steels, whereas newly developed bainitic steels have also been used in heavy-haul rails owing to their superior mechanical properties [1-3]. Compared to ordinary rails, turnouts are loaded not only with haul loads and dynamic rolling contacts, but also impact loads and sliding wear [4-10]. Nowadays the mostly used steels for turnouts include Hadfield steel and low-carbon bainitic steel. Hadfield steel is a high-carbon and high-manganese cast steel known for its excellent impact toughness and work hardening capability, whereas a major drawback is its low strength and low hardness [9, 11]. Bainitic steels developed for rails and turnouts contain carbon up to 0.37 wt% and multiple alloying elements such as Si, Mn, Cr, Ni and Mo [5, 7, 11, 12]. Such compositions were designed to ensure a good combination of toughness and strength properties, while further improvements in the properties can be expected by developing novel strengthening heat treatments [2, 4].

Failure investigation plays a key role in developing new strengthening processes to extend the service lifetime of rails and turnouts. Rolling contact fatigue (RCF) has been identified as the predominant failure mode of rail parts made from pearlitic steels [8], austenitic Hadfield steels [9, 11] and low alloy bainitic steels [1, 6, 9, 11]. Spalling failures developed under RCF loads were found to be attributed to surface strain hardening and subsurface microstructure evolutions [11, 13]. The strain hardening was presented by a gradient depth profile of hardness beneath the worn surface [3, 9]. Luo reported that the subsurface hardness of a failed Hadfield steel turnout was higher in the zones showing spalling cracks than in the crack-free zones [9]. The microstructure evolutions included plastically deformed grain shape, increased density of dislocations and twins, grain refining and laminated structures, as well as quasi-amorphous structures called ‘white-etching layers’ (WEL) [6, 11, 13-16]. Zhang compared the microstructure evolutions of two used turnouts made from Hadfield steel and bainitic steel. Both turnouts exhibited similar spalling failure and severe surface deformation, whereas WEL was observed only in the Hadfield steel turnout [11]. Chen, on the other hand, reported WEL formation in a bainitic steel when the steel was subjected to severe RCF loads [6]. Nguyan reported that the mechanism of WEL formation in a pearlitic steel comprised of severe plastic deformation and the thermal-mechanically induced phase transformation [17]. In addition, the depth-dependent

deformation also led to residual compressive stresses although this phenomenon was reported only in limited cases [9]. For bainitic steels containing austenite, transformation induced plasticity (TRIP) has been reported to contribute to the increased surface hardness [6, 13, 15, 18]. Meanwhile, the TRIP effects were found to result in reduced austenite appearance in the deformed surface when compared to the bulk steels rather than its complete transformation to martensite. Indeed, the direct evidence of austenite to martensite transformation relies on specific analytical techniques, such as transmission electron microscopy (TEM) and related preparation of cross-sectional TEM specimens [9, 15, 19-21]. Recently, we have observed deformation induced acicular martensite in the worn surface of austenitic Hadfield steel [9, 20]. In brief, the published research has revealed the complexity of the spalling failures of rail parts.

In this paper, we report experimental results on failure investigations of an off-track turnout made from bainitic steel. The strain hardening behaviour was characterised using micro-indentation on both the rail surface and subsurface regions, along with surface residual stress measurement. The microstructure evolution in various depths beneath the rail surface, including the TRIP phenomenon, was analysed using optical microscopy (OPM), scanning electron microscopy and transmission electron microscopy as well as X-ray diffraction (XRD). The microstructure evolution has been related to the observed subsurface crack nucleation and propagation, to contribute to an explanation of the deformation induced hardening, embrittlement, and spalling wear failure.

2 Experimental

Failure investigations were undertaken on a used turnout which had been removed from the railway due to spalling failure. The failed turnout was sectioned into pieces for the analysis. A longitudinal piece containing the failed top is shown in Figure 1a. The rail top shows a ridge line in the middle, whereas both sides are arc-shape instead of flat. Both sides, marked 'Side A' and 'Side B' respectively, show evidence of spalling marks along the length. The entire turnout surface was covered with an orange red corrosion product, suggestive of corrosion. The surface corrosion product was removed using an electrolytic method by immersing the sample in a 10% sodium hydroxide solution and applying a current through the samples. The samples were further cleaned with a soft nylon bush to remove any loose corrosion product before being washed in Industrial Methylated Sprits dried and stored in anticorrosion paper, leading to an oxide-free clean rail top as shown in Figure 1b. In Figure 1b, several spalling pits had been formed in addition to other wear features such as cracks.

Several small pieces were cut transversely from the rest part of the longitudinal piece using an abrasive wheel cutter under water-based cooling, for cross-sectional analysis. These samples were prepared following a procedure of mounting in Bakelite, manual grinding on abrasive papers, and metallographic polishing to a mirror finish. The samples for microstructure observations were etched using a 2% nital etchant. Figure 1c shows an example of optical microscopy (OPM) observations of the etched cross-sections, where the surface cracks were seen to have propagated to a depth up to 0.9 mm.

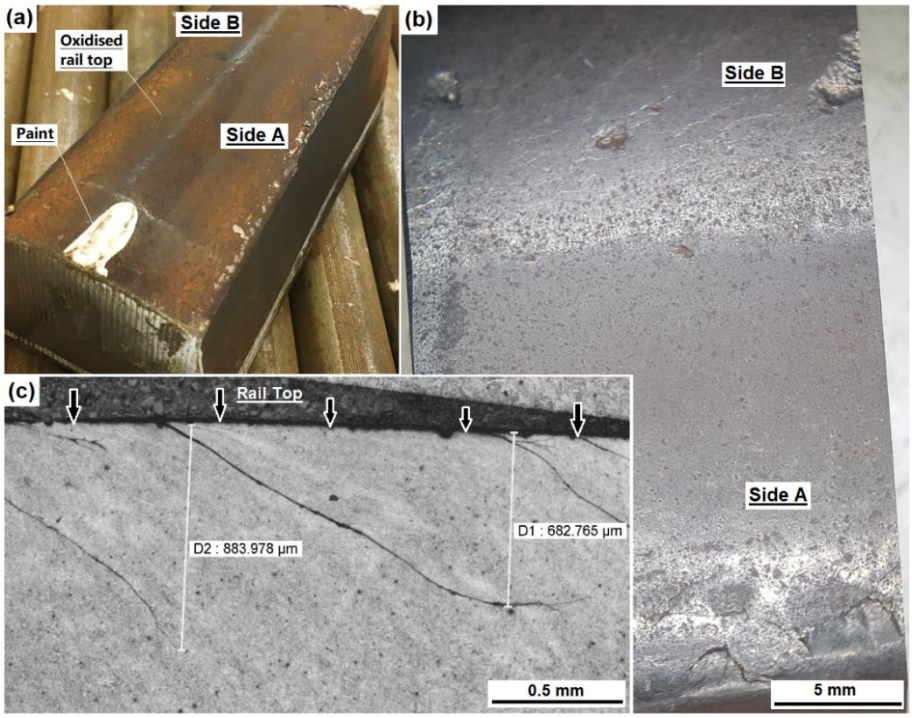

Figure 1 The turnout to be analysed: (a) a photo of the rail top piece as well as several cylindrical bars machined from the bulk turnout; (b) a photo of the electrolytically clean rail top showing large spalling pits; (c) an optical microscopic image of the etched transverse cross-section showing propagation of cracks from the rail top to certain depths. The black arrows in (c) show the position of the rail top.

Tensile and V-notch Charpy impact tests of the bulk metal were carried out at room temperature following the standards BS EN ISO 6892-1-2019 and BS EN ISO 148-1:2016, respectively. The mechanical tests were made in triplicate to obtain the average values and standard deviation. A Struers Duramin-40 AC3 hardness tester was employed to measure the hardness using a Vickers indenter. The Vickers hardness of the bulk steel was measured at a depth of 10 mm below the rail top under an indenting load of 30 kgf (termed as

HV_{30}), being averaged from five measurements. Microhardness measurements were made using a load of 0.1 kgf (termed as $HV_{0.1}$) both on the rail top and on various depths of the cross-section samples to determine wear induced strain hardening severity.

The microstructure of the prepared samples was characterised using several methods, including optical microscopy (OPM), analytical scanning electron microscopy (SEM) with energy dispersive X-ray spectroscopy (EDX), TEM and X-ray diffraction (XRD). The chemical composition of the turnout was analysed using a spark optical emission spectroscope (OES) and SEM-EDX. A field-emission scanning electron microscope was employed both to observe the failure patterns on the as-obtained rail tops and to examine wear induced microstructure on the transverse cross-sections. Further examination of the microstructure evolution was made using a field-emission transmission electron microscope, JEOL 3100F TEM operating at 200 kV. Cross-sectional TEM samples were thinned in a procedure of manual grinding and low-angle argon ion-beam milling, as described in Ref. [22].

An X-ray diffractometer using Co-K_α radiation (wavelength 0.1789 nm) was employed to perform crystallographic analysis of the bulk steel when it was operated under the θ-2θ scan mode and at a scanning speed of $0.009°{\cdot}s^{-1}$. The diffractometer was also employed to measure residual stresses of the failed rail top, which was operated under the σ-2θ scan mode and at a scanning speed of $0.006°{\cdot}s^{-1}$. The residual stresses were measured using a modified $sin^2\psi$ method [23]. The diffraction peaks of ferrite plane F(211) were acquired at a series of off-axis angles (ψ) of 0°, ± 16°, ± 24°, ± 30°, ± 35.2° and ± 40°. The measurements were made to obtain the residual stresses in both the axial and transverse directions and on both sides of the rail top, as shown in Figure 1a. In the calculation of residual stresses, the elastic modulus (E) and Poisson's ratio (ν) were assumed to be 210 GPa and 0.30, respectively [9].

3 Results

3.1 The chemical composition, mechanical properties and microstructure of the bulk steel

Table 1 shows the chemical composition of the turnout. The elemental composition was determined using OES and SEM-EDX methods where the alloying elements of Si, Mn, Cr, Ni and Mo were detected. The concentration of the alloying elements was determined to be comparable for each method. Furthermore, the composition is consistent to the bainitic rail steels reported by other researchers [4, 7, 11]. The steel is similar to the bainitic rail grade as specified in Ref [12] except its higher content of C, Si and Cr. Another exception was the slightly higher content P and S, which was due to the instrumental limitation of SEM-EDX spectroscopy in analysing trace elements in such low concentrations. The low carbon content favoured good toughness, whereas the multiple alloying elements are used to obtain bainitic microstructure under a relatively slow cooling heat treatment.

Table 1 The chemical composition (wt%) of the turnout.

Method	C	Si	Mn	Cr	Ni	Mo	P	S	Fe
OES	0.26	1.51	1.77	1.34	0.27	0.28	Non-detectable		In balance
SEM-EDX	-	1.58	1.86	1.51	0.24	0.22	0.05	0.04	In balance
Ref [12]	0.16 - 0.25	0.7 - 1.2	1.6 - 2.45	0.16 - 1.2	0 - 0.7	0.15 - 0.6	≤ 0.022	≤ 0.015	In balance

Table 2 summarises the mechanical properties of the bulk steel. The values of ultimate tensile strength (σ_m), yield strength (σ_s), area reduction ratio (ϕ) and total elongation (ε) are in a similar scale to those bainitic rail steels reported in literature [4, 7, 11, 13]. The total elongation includes a contribution of uniform elongation (ε_1) of 8%. The hardness and tensile properties meet the technical specifications of U20MnSiCrNiMo bainitic rails [12]. The V-notch Charpy impact toughness (K_V) of the investigated bainitic turnout is much lower than that of the austenitic high-Mn Hadfield steel turnout (197 ± 9 J) measured in our previous work [9]. The great difference is attributed to the excellent plasticity and strain hardening capacity of Hadfield steel. Moreover, it should be noted that impact toughness measured in our current work is not comparable to the toughness property specified in Ref [13] because the V-type and U-type notches are known to contribute differently to the impact fracture.

Table 2 The mechanical properties of the turnout.

Material	HV30	Tensile properties						Impact Energy
		E	σ_m	σ_s	ε	ε_1	ϕ	
	Kg/mm^2	GPA	MPA	MPA	%	%	%	J
This work	420 ± 6	201 ± 1	1281 ± 10	1021 ± 9	18 ± 1	8	54 ± 2	K_v: 35 ± 1
Specification [12]	376 - 458	-	≥ 1280	≥ 1000	≥ 12	-	-	K_u: 70

Figure 2 shows SEM observations of the obtained tensile and impact fractures. Under both testing conditions the steel exhibited microvoid coalescence features, typical of ductile fracture. The tensile fracture in Figure 2a shows fracture normal to the axis in the core part and shear fracture in the outer edge. Further higher magnification observations of the tensile fracture suggest voids-

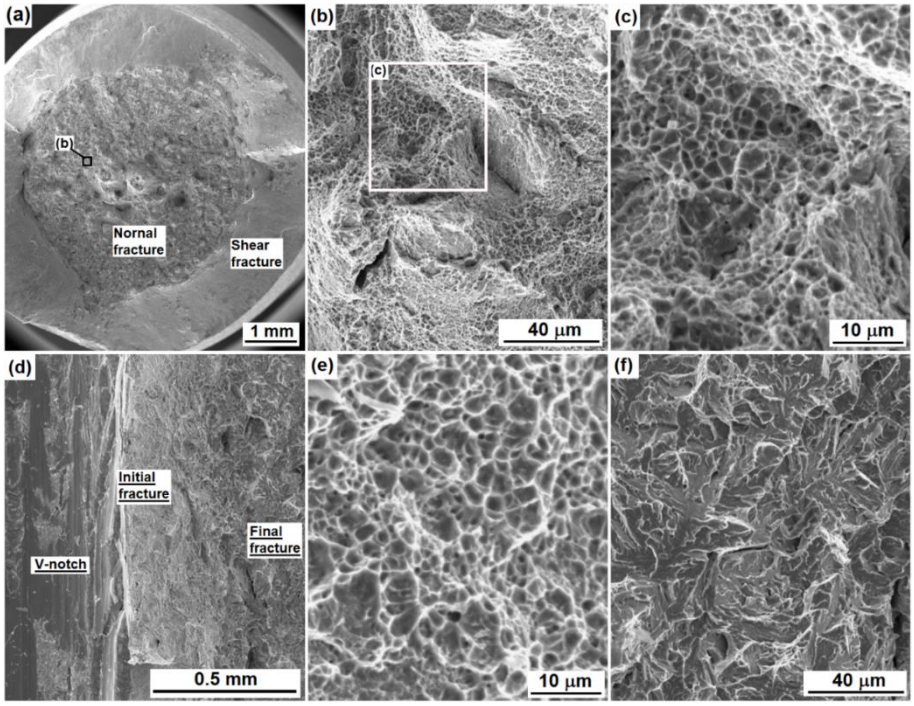

Figure 2 SEM fractographic analyses of tensile and impact samples: (a-c) tensile fracture at various magnifications; (d) V-notch impact fracture at low magnification; (e) voids-type ductile fracture in initial fracture area; and (f) quasi-cleavage fracture in final fracture.

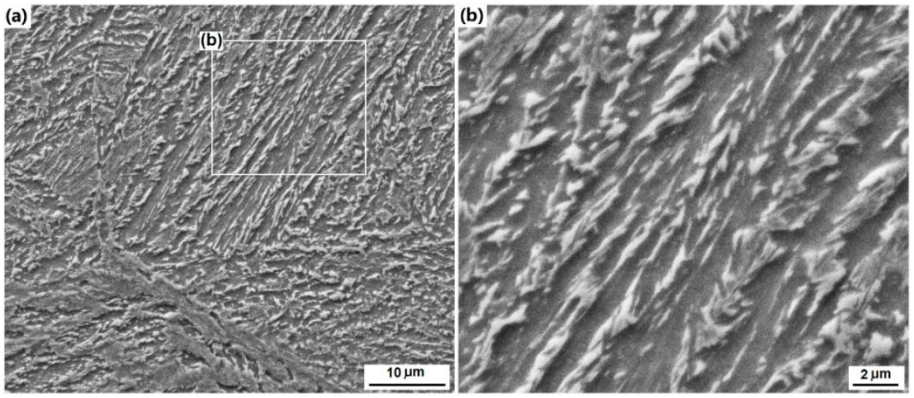

Figure 3 SEM images showing the bulk microstructure of the turnout: (a) the bainitic ferrite matrix and uniform distribution of retained austenite (in bright contrast); and (b) an enlarged image showing lath-like bainitic ferrite and inter-lath austenite.

type ductile fracture, as shown in Figures 2b and 2c. Figure 2d is a low-magnification view of an impact fracture section, where the deformation grooves in the left-hand side show the machined V-type notch. The fracture initially exhibited the ductile voids-type mode, as shown in Figure 2e, followed by a transition to the less-ductile quasi-cleavage mode, as shown in 2f.

Figure 3 shows the microstructure of the bulk bainitic steel about approximately 10 mm beneath the rail top. The steel exhibited a dual-phase microstructure of bainitic ferrite and retained austenite without appearance of any carbide. The inhibition of carbide precipitation should be attributed to the role of silicon as reported by many other researchers [2, 5, 24, 25]. Lath-like bainitic ferrite dominated the microstructure whereas retained austenite showed a morphology of either inter-lath films or blocks.

The dual-phase structure was also determined in XRD analysis, as shown in Figure 4. The bulk steel showed strong peaks of austenite, namely, (111), (200), (220) and (311) peaks. The austenite in the bulk steel was quantified to show a lattice constant of 0.3613 nm and volume fraction of 17.0 %, respectively.

3.2 Analyses of the worn rail top

The rail top and subsurface were analysed using XRD, microhardness testing, SEM observations and spectroscopic techniques to investigate the effect of rolling contact on the steel properties with respect to depth from the rail surface. Changes to the crystallography were investigated where diffraction curves of the worn rail top surface, approximately 0.08 mm beneath the surface (i.e. subsurface), following a polishing process, and with the bulk material were acquired for comparison (Figure 4). Further analysis included investigating rolling contact induced strain hardening by measuring the microhardness on the rail top and at various depths from the worn rail top (Figure 5). Furthermore, the average and standard deviation microhardness of identified areas of the rail turnout i.e. Rail top (cracked), Rail Top (crack free), 0.08 mm, 0.18 mm and 4.0–5.0 mm is presented in the bar chart in Figure 6.

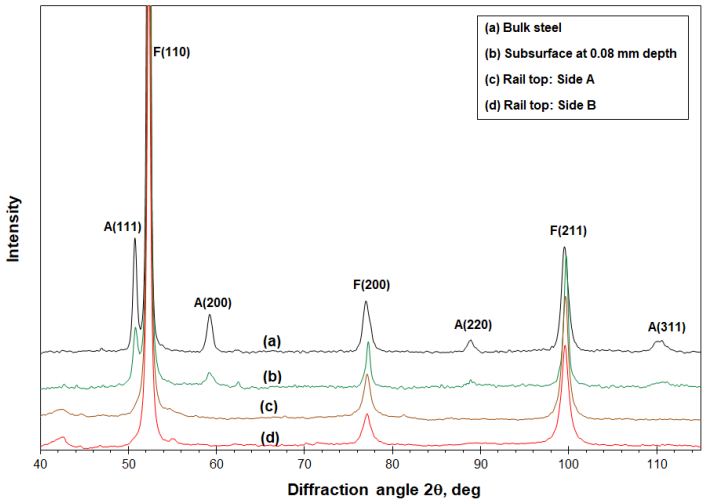

Figure 4 X-ray diffraction curves acquired at various locations: the bulk steel 10 mm beneath the rail top, subsurface at a depth of 0.08 mm, and rail tops on Side A and Side B (from top to bottom).

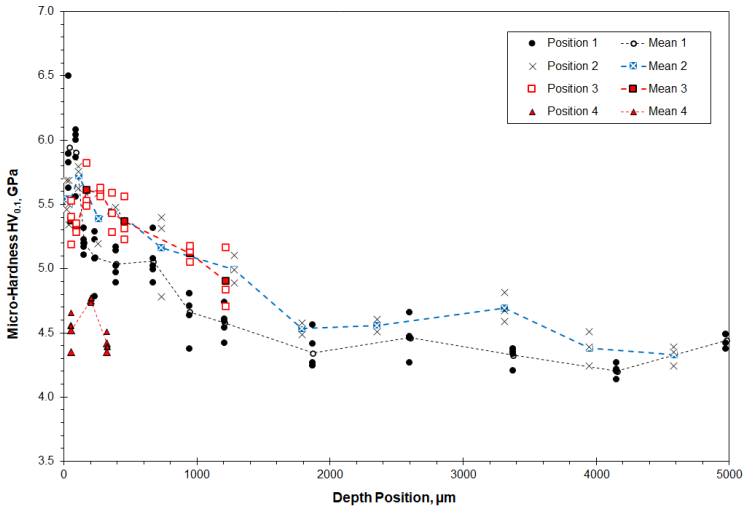

Figure 5 Microhardness plotted versus depth positions of the worn turnout: Position 1 and Position 3 refer to two areas exhibiting severe plastic deformation and cracking; Position 2 refers to an area exhibiting severe deformation but free from cracking; and Position 4 is a place exhibiting only mild plastic deformation and no subsurface cracking.

The diffraction peaks acquired in the bulk steel denote austenite free from plastic deformation, corresponding to a low hardness of HV0.1 4.4 GPa. In contrast, the subsurface area shows decreased diffraction intensity of the austenite peaks. Accordingly, the microhardness measured at the depth of 0.08 mm has increased to HV0.1 5.9 GPa. It is indicated in Figure 5 that significant strain hardening took place up to a depth of 1.4 mm. More interestingly, the upmost worn surface showed no austenite peak at all, suggesting that the amount of retained austenite had become too small to be detected in the XRD acquisition. Furthermore, the maximum hardness was measured in areas where cracking was observed, however in areas that were free from cracks the hardness was lower. The increased hardness and decreased austenite at the rail top suggest that there was deformation induced transformation of the austenite to ferritic structure.

SEM observations were carried out on the rail top of the turnout, as shown in Figure 7. Figure 7a is an overview, where the rail top was found to be full of delamination pits. Several shear edges were marked by white arrows, indicating spalling wear. Macro-scale spalling pits are shown in Figure 7a and were observed at higher magnifications, as shown in Figures 7b and 7c. These features indicate brittle delamination of small fragments.

The shear edges in Figure 7a were related to subsurface cracks as shown in Figure 1c. To clarify this, the arc-shape rail top was flat-ground and polished at a low-angle inclined metallographic cross-section, followed by etching with 2% nital to show the subsurface microstructure within a very small depth range. Figure 8 shows selected results of SEM observations. In Figure 8a, the worn rail top shows a layered structure from the oxidised rail top (marked 'I'), an etching-resistant featureless top layer (marked 'II') and the severely deformed bainitic microstructure containing inter-granular cracks (marked 'III'). Further observation at a higher magnification, as shown in Figure 8c, revealed more details of the different regions at a better spatial resolution. The fine features in most of the imaged areas revealed the binary bainitic ferrite and retained austenite. EDX analyses of typical areas are shown in Figure 9, where the four spectra refer to the regions marked in Figure 8c. Spectrum 1 confirms the metallic nature of the bainitic matrix. However, the matrix had completely lost its regular lath-like morphology of the bulk steel (Figure 3) by exhibiting severe deformed shapes. Spectra 2 and 4 were acquired from the contaminants, indicating that the subsurface cracks and surface spalling pits had accommodated corrosion products as indicated by the higher O and C contents.

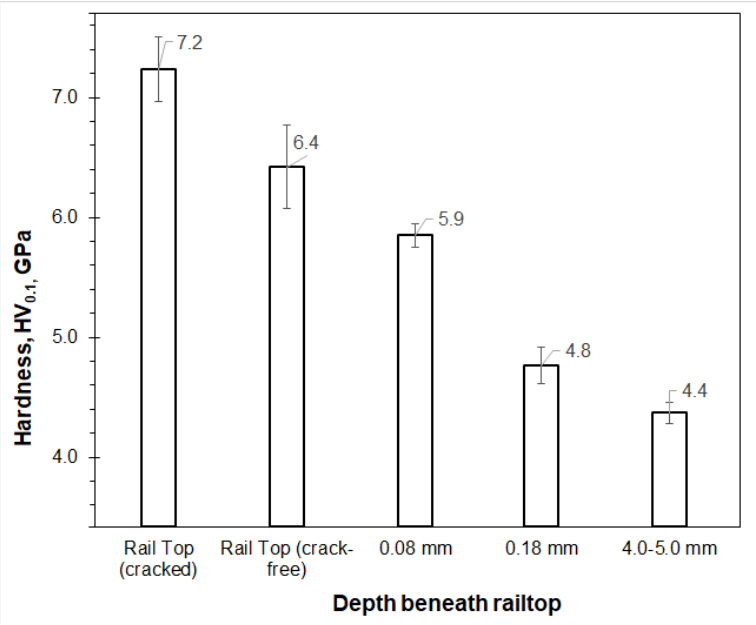

Figure 6 Microhardness property measured at various depths of the worn turnout.

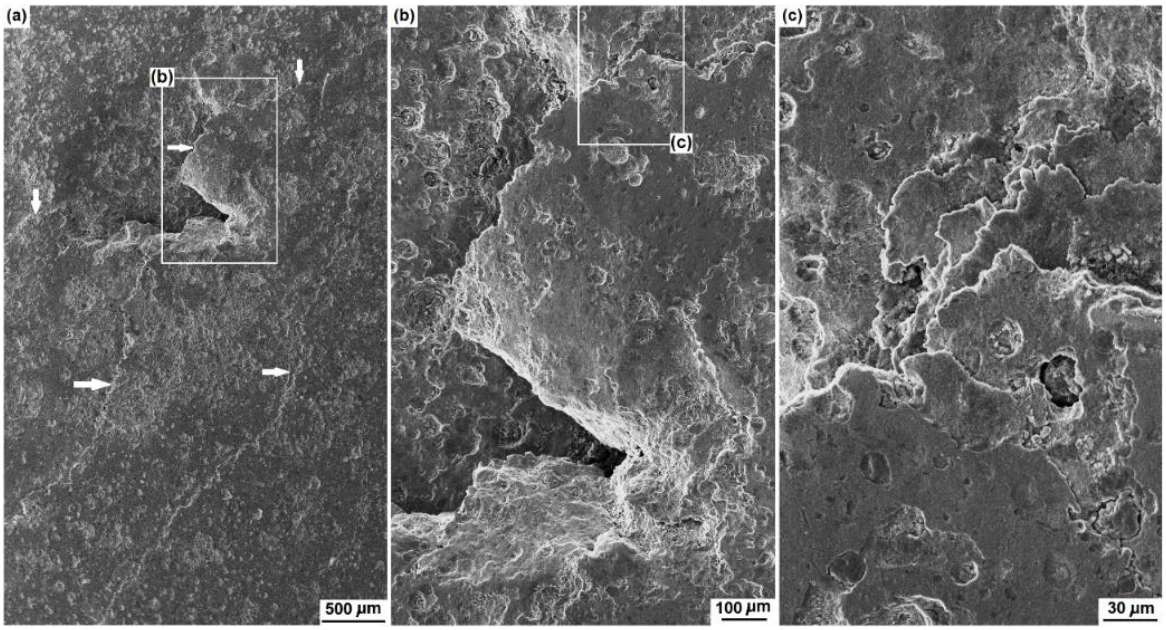

Figure 7 SEM images taken on the worn rail top surface: (a) A low-magnification overview of the relatively smooth worn surface and a spalling site. (b) A high-magnification view from the spalling edge. (c) A further high magnification view of the spalling failure showing brittle fragments on the facet worn surface.

Figures 8b and 8d show microstructure of the turnout at a depth of approximately 50-80 µm beneath the rail top. The morphology of the bainitic ferrite and retained austenite had become significantly disordered as compared to the bulk steel, by comparing between Figures 8d and 3b. Such disordered morphology is an evidence of severe plastic deformation. In addition, inter-granular and trans-granular cracks can be seen to have propagated to such depths, whereas the cracks were filled with corrosion products similar to those observed in Figures 8a and 8c. By comparing the morphology of the bainitic structures shown in Figures 3b, 8c and 8d, it has been demonstrated that the turnout had accumulated depth-dependent plastic deformation.

Moreover, special attention was paid to a feature-less smooth area in Figure 8c. Firstly, the feature-less smooth area is not a part of the oxidised top layer because that the acquired EDX spectroscopy is consistent to the bainitic matrix, essentially free from oxygen (comparing Spectrum 3 and Spectrum 1 in Figure 9). Secondly, the area was feature-less in the SEM imaging as compared to the severely disordered bainite-austenite dual-phase matrix in the adjacent zone. Such feature-less structures were not found in any further depth, such as in the depth of 50 - 80 µm as shown in Figure 8b and 8d. Instead, the feature-less morphology was consistent to the top layer as marked 'II' in Figure 8a. These chemical and morphological features are similar to the so-called 'white-etching layer' or 'white-etching area' as described in literature [6, 8, 10, 11]. Its formation can be explained by that the repeated plastic deformation was extremely severe to have resulted in the regular dual-phase structure to change gradually to a nano-crystalline or quasi-amorphous layer at the outmost rail top.

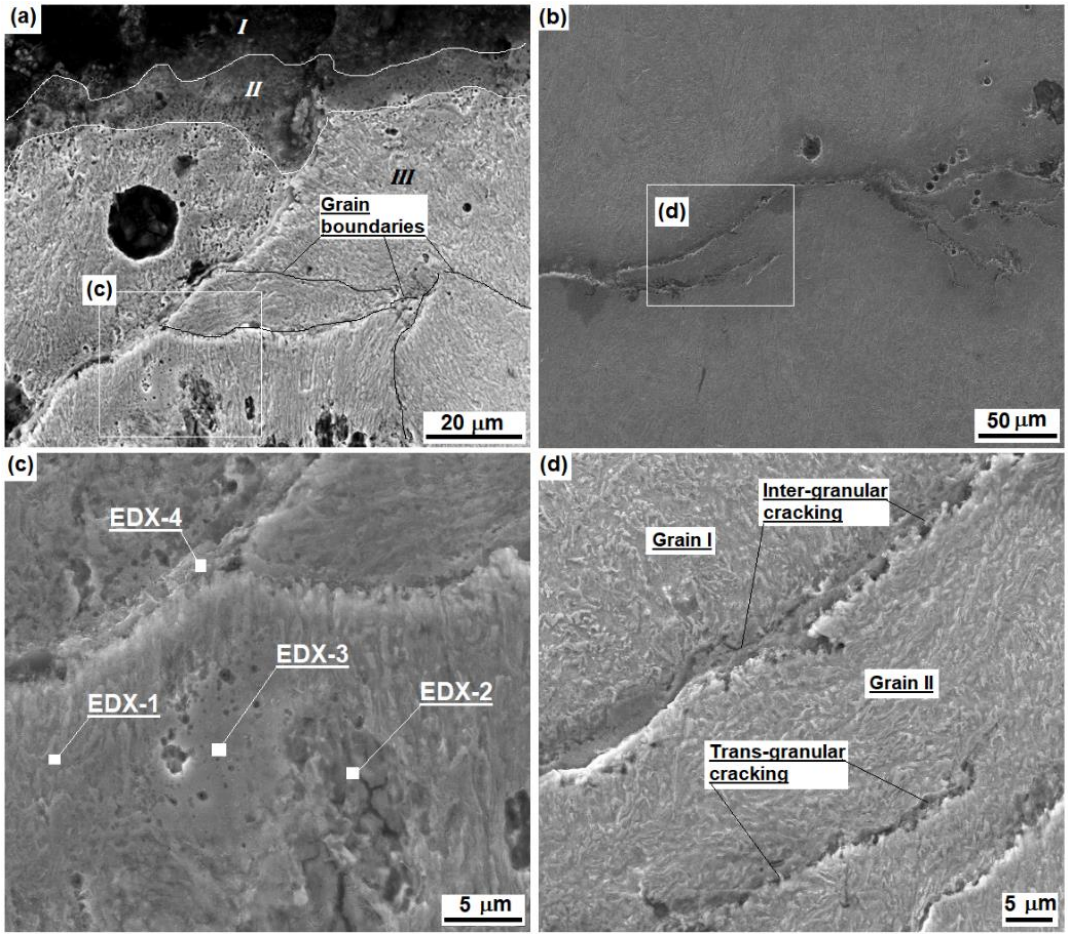

Figure 8 SEM images showing the rail top after metallographic polishing and etching: (a & c) Low-angle inclined cross-sectional observations. (b & d) Severely deformed bainitic microstructure and inter-granular and trans-granular cracks at a depth of approximately 50-80 μm beneath the rail top. The marks 'I', 'II' and 'III' in (a) denote the surface oxide, the etching-resistant rail top and etched bainitic microstructure respectively.

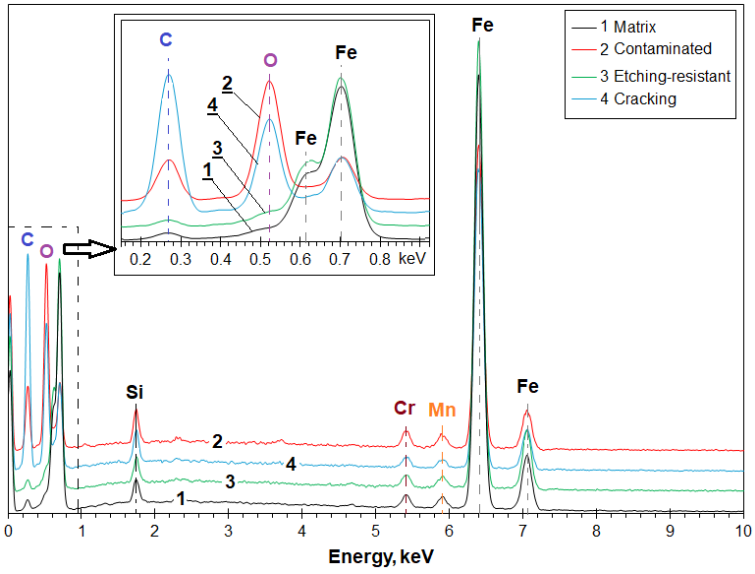

Figure 9 Energy dispersive X-ray spectra of the rail top subsurface. The spectra were acquired at the positions marked in Figure 8c.

Figure 10 shows an example of XRD measurements of residual stresses on both sides of the rail top. The results of residual stress measurements are summarised in Table 3. Residual stresses were primarily in the form of compressive normal stresses as compared to the marginal residual shear stresses. The residual stresses were predominately along the transverse direction of 300 - 410 MPa, but much lower than the yield strength of the bainitic steel and not as severe as those measured on a failed austenitic turnout, i.e., 504 MPa and 648 MPa as reported elsewhere [9]. Nevertheless, the detection of residual compressive stresses provided further evidence of severe plastic deformation accumulated on the rail top.

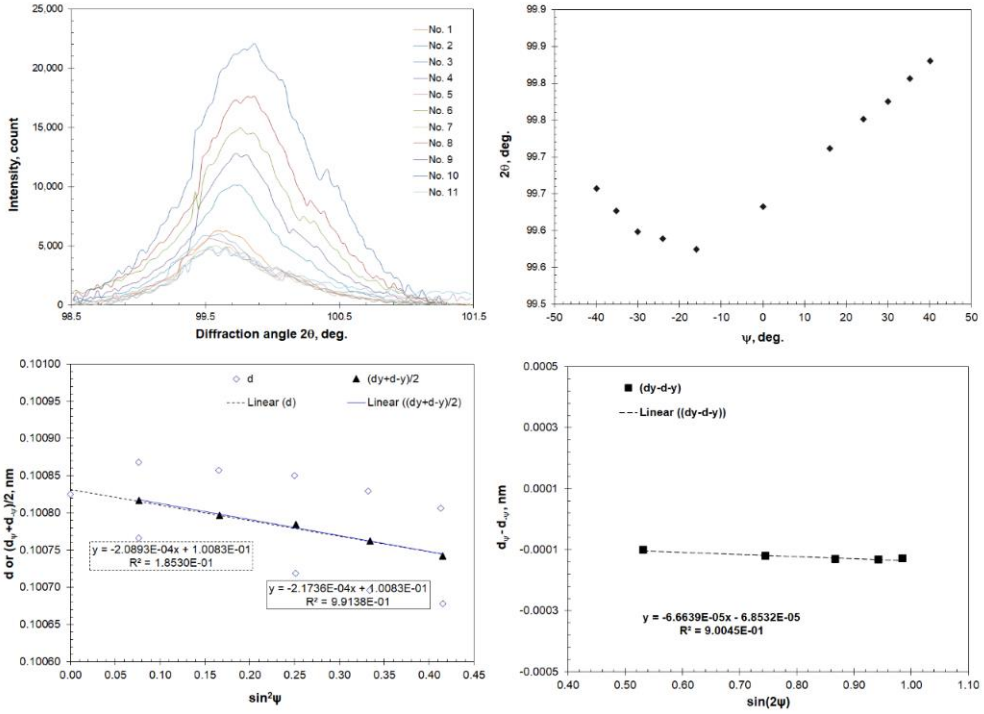

Figure 10 An example of XRD residual stress measurement performed on the rail top: (a) The F(211) diffraction peaks acquired at various off-axis angles (ψ). (2) The measured peak position (2θ) plotted versus off-axis angles (ψ). (c) Linear regressions to calculate normal stress σ. (d) Linear regression to calculate residual shear stress τ.

Table 3 Residual stresses measured on the worn rail top of the failed turnout.

Location	Transverse direction		Axial direction	
	σ (MPa)	τ (MPa)	σ (MPa)	τ (MPa)
Side 'A'	-332 ± 21 -350 ± 36	111 ± 14 28 ± 25	-99 ± 36	13 ± 11
Side 'B'	-409 ± 29	35 ± 16	-275 ± 51	23 ± 22
Hadfield steel [9]	-648 ± 41 -504 ± 35	50 ± 26 50 ± 28		

3.4 Characterisation of deformation induced microstructure evolution

Cross-sectional SEM and TEM were employed to characterise deformation induced microstructure evolution beneath the worn rail top. Figure 11 presents an example of the extensive cross-section SEM observations.

Figure 11a is an overall view of cross-sectional microstructure from the rail top to a depth of 0.22 mm. The most significant deformation took place at the rail top in a depth of approximately 0.05 mm, as indicated by the red dash line. Figure 11b shows further details at a higher magnification, in which the remarkably interrupted microstructure reveals severe plastic deformation. Figures 11c and 11d show further details of the deformed microstructure at the specified depths. In Figure 11c, the upmost microstructure above the dash line had become extremely fine and disordered, including several small cracks as labelled by the black arrows. Further propagation of these cracks would generate a new delamination fragment. Figure 11d shows a high-magnification image at a depth range of 0.02 - 0.04 mm, where the plastic deformation is typically evidenced by the deformed morphology of the austenite (in brighter contrast). In Figure 11e, the bending deformation at a depth of 0.06 - 0.11 mm is recognised only in the marked area whereas the microstructure surrounding that area retains the ordinary bainitic morphology. In the areas of further increased depths, the microstructure exhibits no remarkable morphological variation, as shown in Figure 11f.

Figure 12 shows TEM characterisation of a subsurface region close to the top edge. The bright field image in Figure 12a indicates nano-scale laminar morphology parallel to the worn top surface. The thickness of the laminar grains was measured to be in the range of 55 ± 18 nm. The nano-laminates show sub-structures of dislocation cells with domain dimensions of 40 ± 9 nm. Figure 12b is a selected area diffraction pattern acquired in the observed area. The pattern suggests predominantly bainitic ferrite as well as a trace appearance of retained austenite. In particular, the joint-presence of ferrite and austenite patterns, F(110) and A(111), is shown in the insert. The two patterns are very close to each other because of the similar lattice spacings , i.e., 0.208 nm for A(111) and 0.203 nm for F(110) providing a very small lattice mismatch of 2.5%. Nevertheless, the SAD analysis suggested distinct presence of retained austenite.

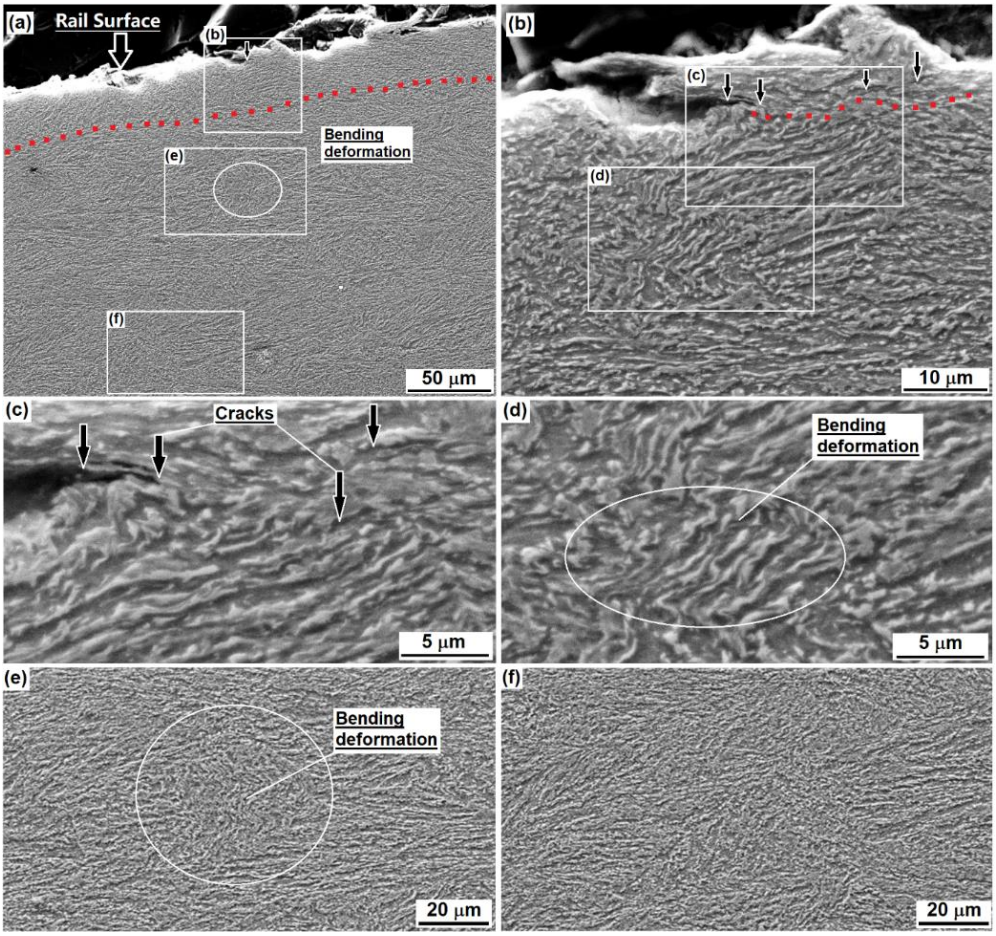

Figure 11 Cross-sectional SEM images showing gradient deformation beneath the rail surface: (a) a low-magnification overview from top to a depth of 0.22 mm. (b) Depth range 0 - 0.05 mm. (c) Depth range 0.01 - 0.02 mm. (d) Depth range 0.02 - 0.04 mm. (e) Depth range 0.06 - 0.11 mm. (f) Depth range 0.16 - 0.21 mm.

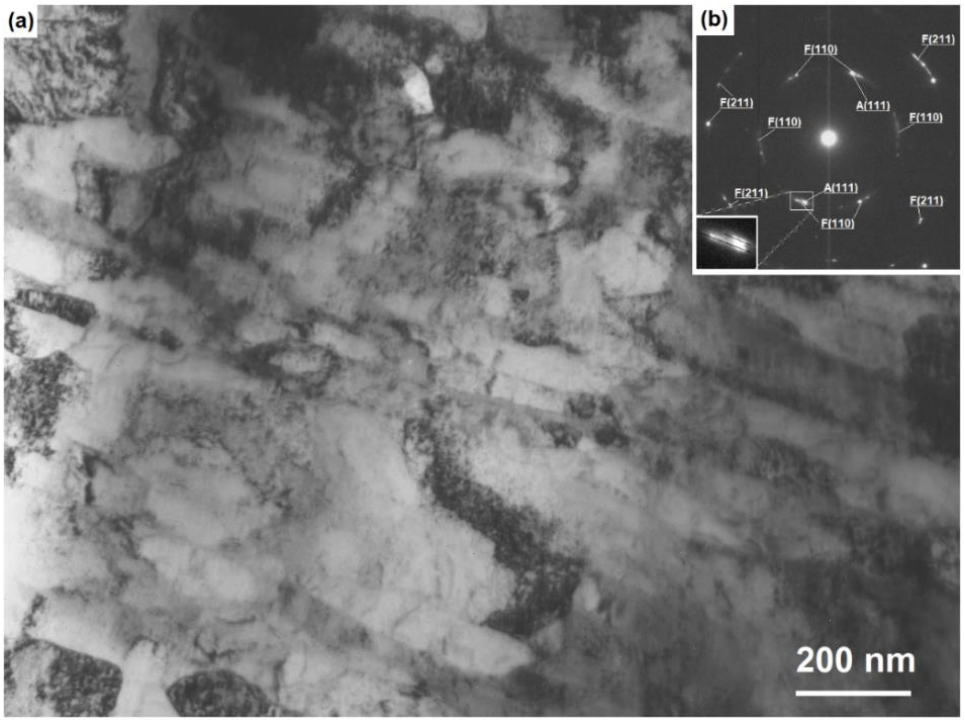

Figure 12 High-resolution observation of the extremely deformed microstructure of the rail top. (a) A bright field TEM image showing the laminated microstructure. (b) A selected diffraction pattern taken in the observed area confirming weak presence of retained austenite along with the majority of bainitic ferrite.

Figure 13 shows TEM observations and related diffraction analysis in a subsurface zone approximately 20 µm beneath the worn surface. This area exhibited equaxial morphology with grain sizes of 229 ± 61 nm. Interestingly, several acicular sub-structures were observed in one of the grain in the imaged area, as highlighted in Figure 13a and further imaged in Figure 13b at a higher magnification. The acicular grains were 61 ± 16 nm in length and 8 ± 2 nm in width. These could be recognised as deformation-induced martensites transformed following a shear mode. SAD patterns obtained in this area show co-existence of austenite and bainitic ferrite. Such acicular-shape martensites were repeatedly observed in this region but not in the regions showing nano-laminar structures. The preferential presence of acicular sub-structures may imply that shearing transformation of martensite took place in austenite grains which have relatively coarse grain sizes.

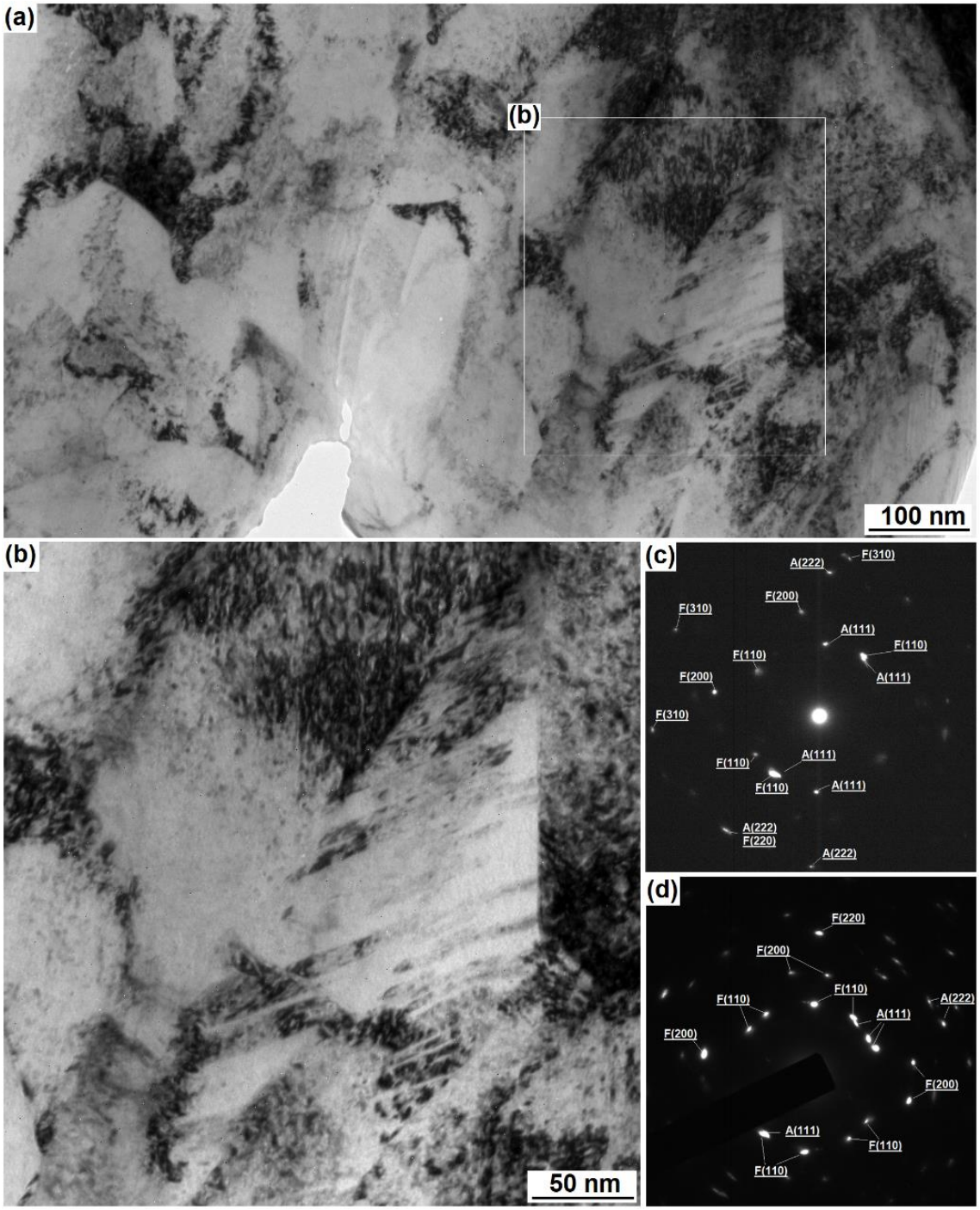

Figure 13 High-resolution observation of deformation induced austenite-to-martensite transformation in close vicinity to the laminated zone. (a-b) Bright field TEM images showing martensite laths formed in an austenite grain. (c-d) Selected diffraction patterns indicating co-existence of ferritic and austenitic phases.

3.5 Cross-sectional observations of subsurface cracking and spalling failures

Extensive SEM observations were applied on metallographically prepared cross-sections of the worn turnout. The observations were focused on the propagation of spalling cracks in the deformation induced gradient subsurface microstructure. Figures 14-16 presents an example of the comprehensive SEM observations.

Figure 14 is spliced low-magnification images, which are separately presented also in Figures 15a and 16a, showing a subsurface crack from its open end on the worn rail top to the growth front. A major crack can be seen to have initiated from the rail surface and propagated to a total length of 970 μm and to a depth of 273 μm below the worn rail top. It grew initially at a low inclined angle of approximately 12° to a depth of 112 μm, and gradually turned to a higher angle of 49.6° before being terminated the maximum depth.

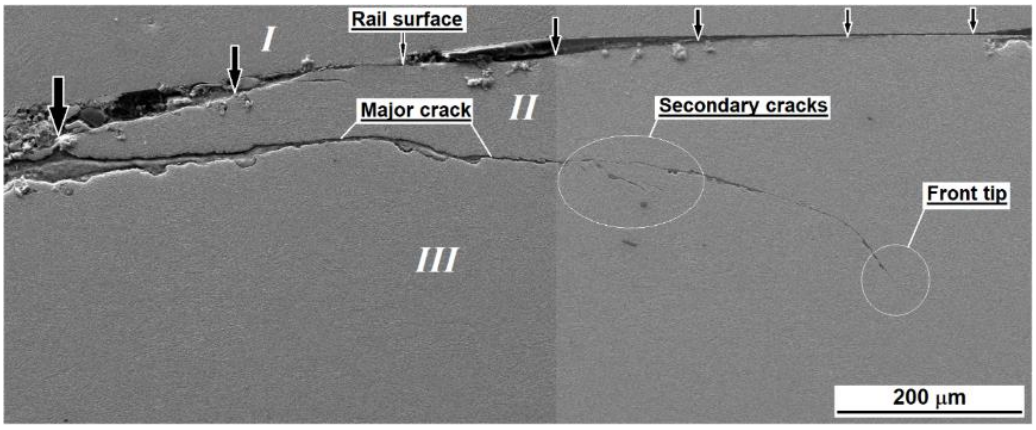

Figure 14 Spliced low-magnification SEM images showing a major spalling crack developed in the deformed depth below the worn rail top surface. The region marked 'I' is a counterpart piece protecting the worn surface from any damage in metallographic grinding and polishing. The labels 'II' and 'III' indicate subsurface regions of the turnout above and beneath a crack. The arrows indicate the rail top.

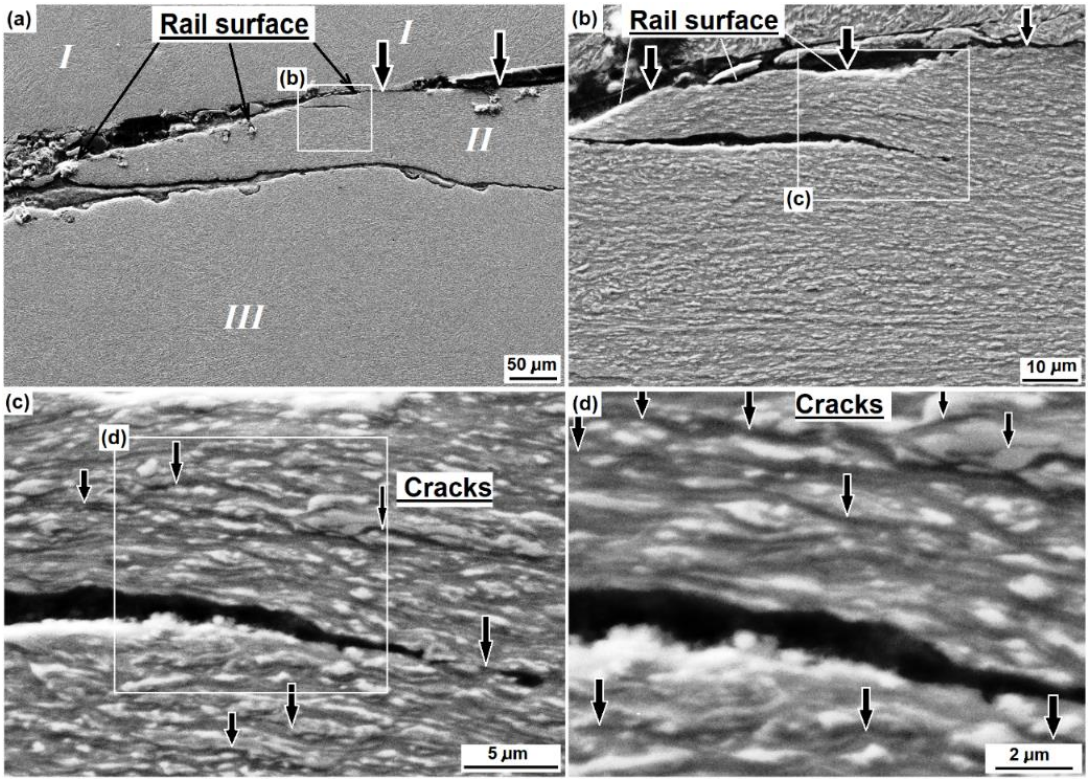

Figure 15 Cross-sectional SEM images showing surface cracking and severely deformed bainitic microstructure. (a) A low-magnification overview of surface cracking following a low inclining angle. (b - d) Further observations of the small crack nucleation-propagation in the depth within the extremely severe deformation region highlighted by the black arrows.

Figure 15a shows the initial growth of the crack to a depth of 112 μm. A small crack, highlighted in Figure 15a and presented at higher magnification in Figure 15b, was found to have nucleated within the severe plastic deformation region a depth of 19 μm . The crack had grown to a length of 75 μm at a shallow angle of 15° with respect to the rail top. Note that the crack propagation followed exactly the laminar orientation, more detailed and higher resolutions images of this region are found in Figures 15c and 15d. Several short

cracks were found within the laminar structure. The crack propagation can be seen to follow the laminar orientation regardless of the bainitic ferrite (having grey contrast), austenite (having bright contrast) or the ferrite-austenite interface.

Figure 16a shows the final section of the major crack adjacent to Figure 15a, in which two selected areas were observed separately at higher magnifications to show details of the deformed microstructure in Figures 16 b-e. The crack follows exactly the laminar orientation in the severely deformed area, as shown in Figures 16b and 16d. Eventually the crack grew into the non-deformed bainitic microstructure at a higher inclination angle. In Figure 16e, it is indicated that the crack propagation was either in the bainitic ferrite or austenite without any preference.

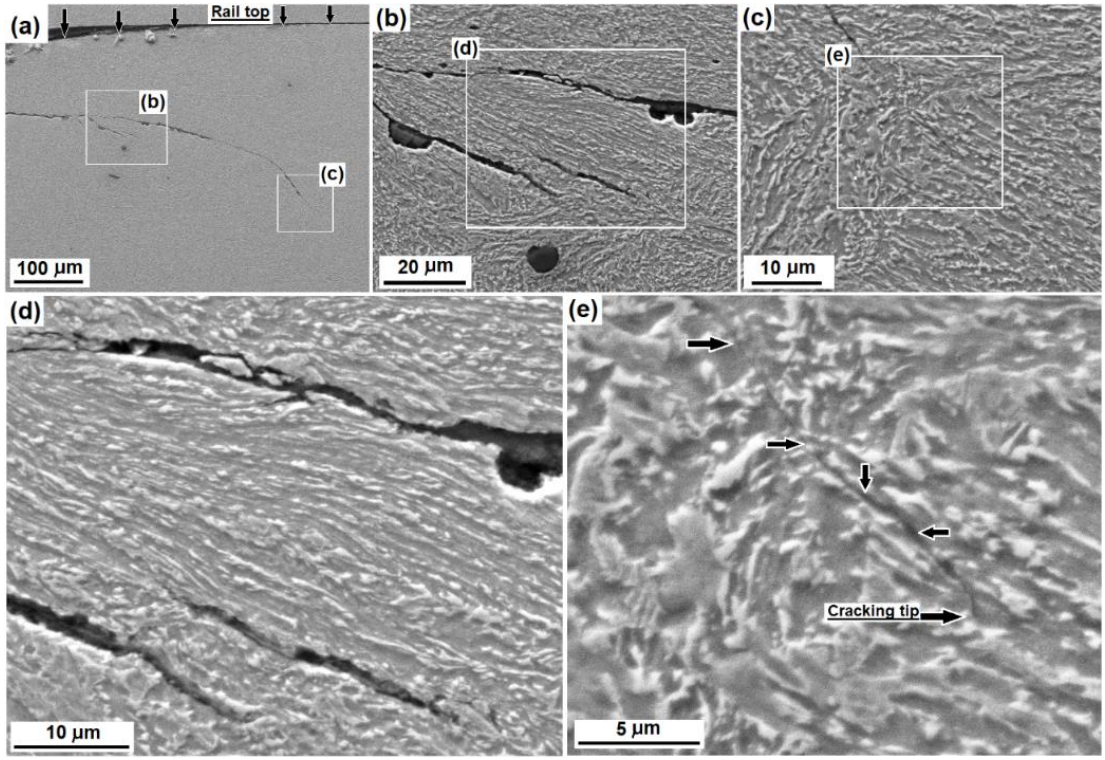

Figure 16 Cross-sectional SEM images showing cracking and deformation beneath the rail surface. (a) A low-magnification view of the section showing a subsurface crack under propagation. (b & d) More details of the cracks and deformed bainitic microstructure. (c & e) The less deformed bainitic microstructure at the front of crack propagation. The black arrows in (e) highlight the crack propagation within the microstructure.

4 Discussion

4.1 The spalling failure mechanisms of bainitic turnout

The spalling wear failure of the investigated turnout was found to include both thin delamination sheets and thick spalling pieces, as shown in Figure 1 and Figure 5. The formation of the small and thin delamination sheets revealed surface embrittlement following the accumulation of plastic deformation and subsequent work hardening of the rail top. The plastic deformation was evidenced by the nano-scale refined laminar-layered microstructure, as shown in Figures 11, 12 and 15. Such severe plastic deformation contributed to the measurement of ultrahigh microhardness along with the formation of a gradient hardness profile from the worn surface to certain depth, as shown in Figures 9 and 10. Crack nucleation and subsequent propagation were found to take place within the severely deformed and embrittled surface layer. In addition, the current work also revealed the formation of high compressive residual stresses in the worn surface. Such in-plane compressive stress is known to trigger a tensile stress perpendicular to the worn surface, which may have also contributed to the crack propagation.

The formation of thick spalling pieces was completed in three steps. Firstly, cracks were nucleated in the rolling/sliding worn surface of the rail top along with the formation of small spalling pits, as shown in Figure 7. The second step is very important as it shows that the cracks grew inside and followed the deformation induced laminar structure to gradually increasing depths, as shown in Figure 14. The severe deformation played a decisive role in promoting the crack propagation due to strain hardening and embrittlement, increased residual stresses and the laminated microstructure. Combined stresses arising from the applied cyclic rolling loads and residual stresses made the cracks propagate into the non-deformed matrix after propagating through the deformed and hardened surface layer, as shown in Figure 16. Finally, the cracks turned growing approximately parallel to the rail top, as shown in Figure 1c. Coalescence of these cracks eventually led to the formation of thick spalling pieces.

In addition, the cracks leading to thick spalling pieces may also bring about a risk of catastrophic failure depending on the strength and toughness properties and on the applied rolling and impact loads. Because of the increased depth, plastic strain in front of the crack

tips could be more restricted to make the local stress-strain to approach to a quasi-plane-strain condition. In such circumstances, sufficiently high toughness is demanded to prevent the occurrence of catastrophic failure.

4.2 Evolution of bainitic microstructure induced by wheel-on-rail rolling contacts

High cycles of wheel-on-rail rolling contacts resulted in significant microstructure evolution on the rail top of the turnout. Cross-sectional examinations revealed a gradient profile of the microstructure and microhardness property from the bulk steel towards the rail top. No remarkable morphological change was observed in the microstructure at the depth of 0.16 - 0.21 mm, whereas bending deformation of bainitic laths had taken place in some grains at the depth of 0.06 - 0.11 mm. At a depth of 0.02 – 0.04 mm from the rail top, the microstructure had become severely laminated with greatly refined thickness and extended length, followed by the extremely fine nanoscale laminates in close vicinity of the rail top. Accordingly, the resultant work-hardening had made the surface hardness to exceed $HV_{0.1}$ 7.3 GPa. Such extreme hardening induced by wear or rolling contacts were also found on the rails made from austenitic Hadfield steel [9] and pearlitic steels [8, 16, 26], as well as on the worn surfaces of Hadfield steel [20] and bainitic steels [13, 21], but was rarely reported in bainitic rails [1, 11, 27].

The current work has also found that, the surface-intensive plastic deformation had promoted a residual compressive stress as high as a scale of 400 MPa, similar to those generated by other means of surface-intensive deformation such as shot-peening [28]. In addition to the expected strengthening against fatigue fracture of shot peened parts, however, the rolling induced residual compressive stresses may have accelerated the subsurface crack propagation and subsequent spalling failure. To our knowledge, few quantitative measurements of residual stresses on worn turnouts and rails have been published [9, 29, 30]. Nevertheless, the measurements provide complementary explanation of the failure mechanisms. Thus, the spalling failures were believed to have been attributed to the deformation, work hardening and associated embrittlement, and high residual compressive stresses.

4.3 New findings on transformation induced plasticity of the bainitic steel

The current work has provided new evidence on deformation induced austenite-to-martensite transformation in the steel having bainitic ferrite and austenite dual phase microstructure. Firstly, XRD analysis revealed greatly minimised levels of austenite on the worn rail top as compared to the subsurface and core of the turnout steel. This finding is consistent to the XRD analysis of many other researchers reporting deformation induced transformation in martensitic and bainitic steels [1, 18, 31, 32]. Complementary to that, the current SEM microstructure observation and TEM-SAD analysis found more details of the transformation behaviour where some retained austenite still survived in close vicinity beneath the worn surface, as shown in Figures 6 and 12. It was unfortunate that the cross-sectional TEM failed to observe the microstructure of the etching-resistant layer. It seems that such extremely deformed and disordered layer contained no or very marginal austenite according to the XRD examination. In literature, such etching-resistant structures were often termed as 'white-etching-layer' and repeatedly found to be quasi-amorphous or nano-equaxial regardless of their crystalline structures [6, 11, 17]. Obviously, further TEM based analysis would be of high interests to verify the complete disappearance of austenite.

Another important finding was the TEM observations of acicular-shape structures providing direct evidence of austenite to martensite transformation under the shear mode. In particular, such acicular martensites were only found in the granular microstructure adjacent to the laminated zone but not within the laminated zone. This finding reveals that such shear transformation took place kinetically only in austenite grains of sufficiently large sizes.

Nevertheless, deformation induced austenite-to-martensite transformation was found to occur under cyclic rolling loads, which implies gradually increased embrittlement of the rail top as shown in the observed spalling failure and subsurface cracks. To improve the resistance to such spalling failures, an important consideration would be to obtain high-strength bainitic microstructure having highly stabilised retained austenite. This scope has been achieved in the research and development of carbide-free bainitic steels which especially showed preferential carbon enrichment in filmy austenite [4, 5, 7, 27, 32]. Consequently, the newly developed bainitic steels promise improved performance in rail applications [7, 14, 15, 18].

5 Conclusions

In this paper, a comprehensive failure investigation has been conducted on the spalling failure mechanism of an off-track bainitic turnout. The experimental research was completed by using optical microscopy, microhardness testing, scanning electron microscopy, energy dispersive X-ray spectroscopy, transmission electron microscopy and quantitative X-ray diffraction. The following conclusions have been made.

1) The turnout was a low carbon and Si-Mn-Cr-Ni-Mo alloyed steel showing a dual-phase carbide-free microstructure of bainitic ferrite laths and retained inter-lath austenite.
2) Two types of wear failures were found, including delamination wear forming micro-scale thin delamination sheets in the severely deformed worn surface and large-scale spalling wear due to surface crack nucleation followed by crack propagation in depths up to 0.9 mm beneath the worn surface.
3) The delamination wear was associated with worn surface embrittlement as a sequence of rolling induced surface deformation, work hardening and the creation of a compressive stress of 400 MPa. The deformation was evidenced by a gradient profile of microstructure evolution a depth of 200 μm, from the bulk steel towards the worn rail top with the formation of a thin etching-resistant shell and a subsurface layer of nano-laminate. The surface work hardening was presented with a gradient microhardness profile to a depth of 1.5 mm, from $HV_{0.1}$ 7.3 GPa of the rail top to $HV_{0.1}$ 3.9 GPa of the bulk steel.

4) Phenomena of transformation induced plasticity (TRIP) were found, not only including the greatly reduced austenite in the laminate structure, but also the formation of martensitic laths beneath the laminates.

Acknowledgements

The authors thank Dr Qintai Yan and Mr Qingpeng Shi (China Railway High-Tech Industry Corporation Limited) for their contributions in setting up the research project, and Mr Dawei Zhang and his colleagues (China Railway Baoji Bridge Group Co. Ltd) for their contributions in selection of failure turnouts. Mr Leon Bowen (Durham University, UK) is acknowledged for the help in TEM analysis. Element Materials Technology (Rotherham, UK) is acknowledged for conducting the mechanical tests.

References

[1] K. Wang, Z. Tan, C. Cheng, B. Gao, G. Gao, R. D. K. Misra, B. Bai, Effect of microstructure on the spalling damage in a 20Mn2SiCrMo bainitic rail, Eng. Failure Analysis, 70 (2016) 343-350.
[2] S. Sharma, S. Sangal, K. Mondal, Wear behaviour of bainitic rail and wheel steels, Mater. Sci. Technol. 32 (2016) 266-274.
[3] W. Wang, R. Song, S. Peng, Z. Pei, Multiphase steel with improved impact-abrasive wear resistance in comparison with conventional Hadfield steel, Mater. Design 105 (2016) 96-105.
[4] A. Kumar, S. K. Makineni, A. Dutta, C. Goulas, M. Steenbergen, R. H. Petrov, J. Sietsma, Design of high strength and damage-resistant carbide-free fine bainitic steels for railway crossing applications, Mater. Sci. Eng. A 759 (2019) 210-223.
[5] O. Hajizad, A. Kumar, Z. Li, R. H. Petrov, J. Sietsma, R. Dollevoet, Influence of microstructure on mechanical properties of bainitic steels in railway applications, Metals 9 (2019) 778.
[6] Y.D. Chen, R.M. Ren, X.J. Zhao, C.H. Chen, R. Pan, Study on the surface microstructure evolution and wear property of bainitic rail steel under dry sliding wear, Wear 448 (2020) No. 203217.
[7] B. Adamczyk-Cieslak, M. Koralnik, R. Kuziak, K. Majchrowicz, J. Mizera, Studies of bainitic steel for rail applications based on carbide-free, low-alloy steel, Metall. Mater. Trans 52A (2021) 5429-5442.
[8] W. Bai, L. Zhu, P. Wang, Y. Hu, W. Wang, H. Ding, Z. Han, X. Xu, M. Zhu, Damage behaviour of heavy-haul rail steels used from the mild conditions to harsh conditions, Wear 496497 (2022) 204290.
[9] Q. Luo, M. Kitchen J. Li, W. Li, Y. Li, Experimental investigation on the spalling failure of a railway turnout made from Hadfield steel, Wear 523 (2023) 204779.
[10] M. Freisinger, B. Jakab, Pichelbauer, G. Trummer, K. Six, P. H. Mayrhofer, Fatigue crack initiation in the presence of stratified surface layers on rail wheels, Int. J. Fatigue 177 (2023) 107958.
[11] F. Zhang, B. Lv, C. Zheng, M. Zhang, S. Yang, Z. Yan, Failure mechanism and worn surface microstructure of high manganese steel and bainite steel crossings, Chinese Journal of Mechanical Engineering, 44 (2008) 232-238.
[12] Technical Specification of U20Mn2SiCrNiMo Bainitic Rails, TJ/GW117-2013, China Railway Press, Beijing, February 2014.
[13] R. Zhang, C. Zheng, C. Chen, B. Lv, G. Gao, Z. Yang, Y. Yang, F. Zhang, Study on fatigue wear competition mechanism and microstructure evolution on the surface of a bainitic steel rail, Wear 482-483 (2021) 203978.
[14] C. Zheng, B. Lv, F. Zhang, Z. Yang, J. Kang, L.She, T. Wang, A novel microstructure of carbide-free bainite medium carbon steel observed during rolling contact fatigue, Script Mater 114 (2016) 13-16.
[15] B. Liu, X. Lu, W. Li, X. Jin, Enhanced wear resistance of nanotwinned austenite in higher Si nanostructured bainitic steel, Wear 398-399 (2018) 22-28.
[16] J. I. Pereira, G. Tressia, E. J. Kina, A. Sinatora, R. M. Souza, Analysis of subsurface layer formation on a pearlitic rail under heavy haul conditions: spalling characterisation, Eng. Fatigue Analysis 130 (2021) 105549.
[17] B. H. Nguyen, A. Al-Juboori, H. Zhu, Q. Zhu, H. Li, K. Tieu, Formation mechanism and evolution of white etching layers on different rail grades, Int. J. Fatigue, 163 (2022) 107100.
[18] A. M. Gola, M. Ghadamgahi, S. W. Ooi, Microstructure evolution of carbide-free bainitic steels under abrasive wear conditions, Wear 376-377 (2017) 975-982.
[19] F. Katsuki, Subsurface characterization of a Fe-0.4 wt%C martensitic steel abraded with nanoindentation and cross-sectional TEM techniques, Wear 303 (2013) 92-97.
[20] Q. Luo, J. Zhu, Wear property and wear mechanisms of high-manganese austenitic Hadfield steel in dry reciprocal sliding, Lubricants 10 (2022) 37.
[21] Z. Zhu, J. Liu, B. Gong, J. Zhao, M. Yang, L. Chen, Analysing the effect of the mechanical stability of residual austenite on the wear performance, Tribo. Int. 192 (2024) 109326.
[22] Q. Luo Q, Electron microscopy and spectroscopy in the analysis of friction and wear mechanisms, Lubricants 6 (2018) 58.
[23] Q. Luo, A modified X-ray diffraction method to measure residual normal and shear stresses of machined surfaces, Int. J. Adv. Manufact. Technol. 119 (2022) 3595-3606.
[24] M. K. Kang, Y. Q. Yang, X. Y. Zhang, J. L. Sun, F. S. Jia, X. L. Wu, Bainitic transformation in silicon-containing steels, Acta Metall. Sin. 32 (1996) 897-903.
[25] F. B. Yang, B. Z. Bai, D. Y. Liu, K. D. Chang, D. Y. Wei, H. S. Fang, Microstructure and properties of a carbide-free bainite/martensite ultrahigh strength steel, Acta Metall. Sin. 40 (2004) 296-300.
[26] S. Li, J. Wu, R. H. Petrov, Z. Li, R. Dollevoet, J. Sietsma, 'Brown etching layer': A possible new insight into the cracking initiation of rolling contact fatigue in rail steels? Eng. Failure Analysis 66 (2016) 8-18.
[27] W. Solano-Alvarez, E.J. Pickering, M.J. Peet, K.L. Moore, J. Jaiswal, A. Bevan, H.K.D.H. Bhadeshia, Soft novel form of white-etching matter and ductile failure of carbide-free bainitic steels under rolling contact stresses, Acta Mater. 121 (2016) 215-226.
[28] J. C. Villegas, L. L. Shaw, K. Dai, W. Yuan, J. Tian, P. K. Liaw, D. L. Klarstrom, Enhanced fatigue resistance of a nickel-based hastelloy induced by a surface nanocrystallization and hardening process. Philos. Mag. Lett. 85 (2005) 427-438.
[29] H.M. Guo, W.J. Wang, T.F. Liu, J.H. Liu, J. Guo, Q.Y. Liu, Analysis of damage behaviour of heavy-haul railway rails, Chinese Mechanical Engineering 25 (2014) 267-272.
[30] S. Dhar, M.K. Danielsen, R. Xu, Y. Zhang, F.B. Grumsen, C Rasmussen, D.J. Jensen, Residual strain-stress in manganese steel railway crossing determined by synchrotron and laboratory X-rays, Mater Sci Technol 37 (2021) 6-13.
[31] S. Balos, D. Rajnovic, M. Dramicanin, D. Labus, O. Eric-Cekic, J. Grbovic-Novakovic, L. Sidjanin, Abrasive wear behaviour of ADI materials with various retained austenite content, Int. J. Cast Met. Res. 29 (2016) 187-193.
[32] B. Narayanaswamy, P. Hodgson, I. Timokhina, H. Beladi, The impact of retained austenite characteristics on the two-body abrasive wear behaviour of ultrahigh strength bainitic steels, Metall. Mater. Trans. 47A (2016) 4883 – 4895.